# Design Optimization of Quarter-car Models with Passive and Semi-active Suspensions under Random Road Excitation

G. VERROS
S. NATSIAVAS
*Department of Mechanical Engineering, Aristotle University, 54 124 Thessaloniki, Greece (natsiava@auth.gr)*

C. PAPADIMITRIOU
*Department of Mechanical and Industrial Engineering, University of Thessaly, 38 334 Volos, Greece*

(Received 28 March 2003; accepted 4 January 2005)

*Abstract:* A methodology is presented for optimizing the suspension damping and stiffness parameters of nonlinear quarter-car models subjected to random road excitation. The investigation starts with car models involving passive damping with constant or dual-rate characteristics. Then, we also examine car models where the damping coefficient of the suspension is selected so that the resulting system approximates the performance of an active suspension system with sky-hook damping. For the models with semi-active or passive dual-rate dampers, the value of the equivalent suspension damping coefficient is a function of the relative velocity of the sprung mass with respect to the wheel subsystem. As a consequence, the resulting equations of motion are strongly nonlinear. For these models, appropriate methodologies are first employed for obtaining the second moment characteristics of motions resulting from roads with a random profile. This information is next utilized in the definition of a vehicle performance index, which is optimized to yield representative numerical results for the most important suspension parameters. Special attention is paid to investigating the effect of road quality as well as on examining effects related to wheel hop. Finally, a critical comparison is performed between the results obtained for vehicles with passive linear or bilinear suspension dampers and those obtained for cars with semi-active shock absorbers.

*Key Words:* Quarter-car models, dual-rate damper, sky-hook damping, wheel hop, stochastic optimization

## 1. INTRODUCTION

Single-degree-of-freedom or two-degrees-of-freedom quarter-car models, subjected to road excitation, are commonly employed in many areas of the automotive industry. These areas include the prediction of dynamic response, identification, optimization and control of ground vehicles (e.g. Karnopp et al., 1974; Harrison and Hammond, 1986; Sharp and Hassan, 1986; Hrovat, 1993; Dixon, 1996; Metallidis et al., 2003). This is mostly due to the simplicity of the quarter-car models and the qualitatively correct information they provide,

*Journal of Vibration and Control,* **11:** 581–606, 2005 DOI: 10.1177/1077546305052315

especially for ride and handling studies. Also, information extracted from such simple models provides quite frequently a firm basis for more exhaustive, accurate, and comprehensive studies with more involved dynamical car models (Verros et al., 2000a).

The main objective of the present study is to develop and apply a systematic methodology leading to optimum combinations of the suspension damping and stiffness parameters of a ground vehicle subjected to random road excitation. Most of the previous studies on the subject have dealt with car models possessing linear characteristics or mechanical models subjected to deterministic road excitation. Moreover, little attention has been paid to revealing and studying important effects related to wheel hop phenomena, mainly due to the inherent difficulty associated with their mathematical modeling (Palkovics and Venhovens, 1992; Verros and Natsiavas, 2001).

The present work combines and integrates recent developments referring to response and optimization of nonlinear quarter-car models, subjected to road excitation. In particular, the models examined involve suspensions with strongly nonlinear damping and stiffness properties and allow wheel hop. Moreover, the road irregularities are assumed to be of random nature and they are described by frequency spectra, which are considered as typical in automotive engineering (Dodds and Robson, 1973; Gillespie, 1992). This excitation is then applied to two-degrees-of-freedom quarter-car models with linear or bilinear shock absorbers and linear or trilinear suspension springs. Specifically, besides linear models, car systems with passive or semi-active dual-rate suspension dampers are also examined. For the last case, a control strategy is applied, based on a choice of the suspension damping coefficient, so that the vehicle approaches a desirable state of sky-hook. In cases where the damping or the stiffness coefficient is variable, the analysis becomes complicated because the resulting equations of motion involve strong nonlinearities. Similar nonlinearities are also introduced even for the linear models, when wheel hop is included in the formulation (e.g. Verros and Natsiavas, 2001).

After selecting the road excitation spectra, the probabilistic characteristics of the response of the nonlinear vehicle models examined are evaluated using Monte Carlo simulations. Sample functions of the random road profile are generated using the spectral representation method and the response of the vehicle to each sample road profile is then computed by integrating the equations of motion (Shinozuka, 1972). The second moment characteristics of the response are finally estimated using the resulting sample vehicle response time histories. These characteristics, in turn, form a basis that is necessary for the development of a computationally appropriate and efficient optimization process.

The material of the present paper is organized as follows. In the next section, we present both the passive and semi-active quarter-car models examined. In Section 3, we present a methodology for computing the second moment characteristics of the response of the nonlinear vehicle models subjected to random road profiles with known spectra. This information is used in Section 4 to define the vehicle performance index that involves quantities related to ride comfort, vehicle handling, and working space of the suspension. Then, a methodology is developed for selecting the optimum values of the suspension damping and stiffness parameters based on that performance index. In Section 5, some typical numerical results are presented, obtained by application of the methodology developed. Emphasis is put on a critical comparison of the results obtained for the linear, the bilinear, and the sky-hook car models. Finally, the highlights of the work are summarized in the last section.

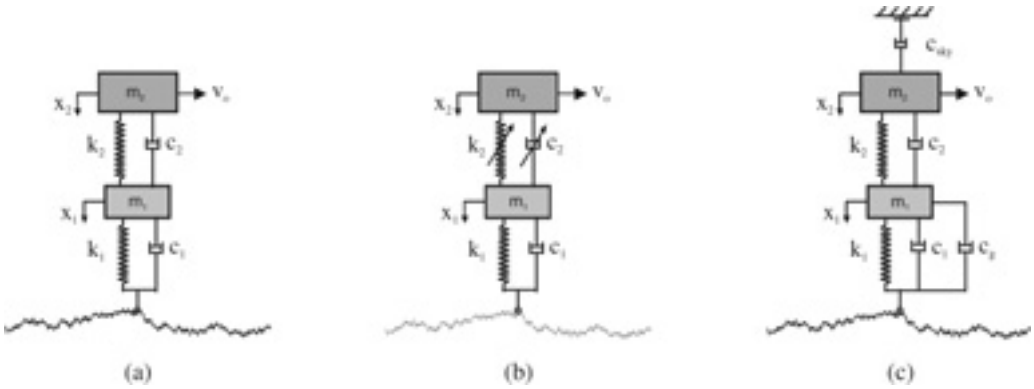


Figure 1. Vehicle models: (a) linear model, (b) piecewise linear model, and (c) sky-hook model.

## 2. MECHANICAL MODELS

The mechanical models of the vehicle systems examined in the present study are shown in Figure 1. They are known as quarter-car models and they are widely used in automotive engineering due to their simplicity and the qualitatively correct information they provide, at least in the initial design stages (Hrovat, 1993). In all cases, the coordinates $x_1$ and $x_2$ represent the absolute vertical displacement of the wheel subsystem and the vehicle body, respectively.

First, for the linear model of Figure 1(a), the equations of motion can easily be put in the classical matrix form

$$M\underline{\ddot{x}} + C\underline{\dot{x}} + K\underline{x} = \underline{f}(t), \tag{1}$$

where $\underline{x}(t) = (x_1 \;\; x_2)^{\mathrm{T}}$ represents the response vector, while the quantities

$$M = \begin{bmatrix} m_1 & 0 \\ 0 & m_2 \end{bmatrix}, \quad C = \begin{bmatrix} c_1 + c_2 & -c_2 \\ -c_2 & c_2 \end{bmatrix} \quad \text{and} \quad K = \begin{bmatrix} k_1 + k_2 & -k_2 \\ -k_2 & k_2 \end{bmatrix}$$

represent the mass matrix, the damping matrix, and the stiffness matrix of the system, respectively. Moreover, the vector $\underline{f}(t)$ includes the forcing terms, arising from the road roughness. In particular, the vehicle is assumed to travel with a constant horizontal velocity $v_0$ over a road with a profile $s(z)$. Here, this profile is represented by a random process with a statistical distribution, which is consistent with measurements of typical road profiles (Dodds and Robson, 1973). Therefore, the forcing vector is expressed in the form

$$\underline{f}(t) = \begin{pmatrix} k_1 x_g(t) + c_1 \dot{x}_g(t) + m_1 g \\ m_2 g \end{pmatrix},$$

where $x_g(t) = s(v_0 t)$.

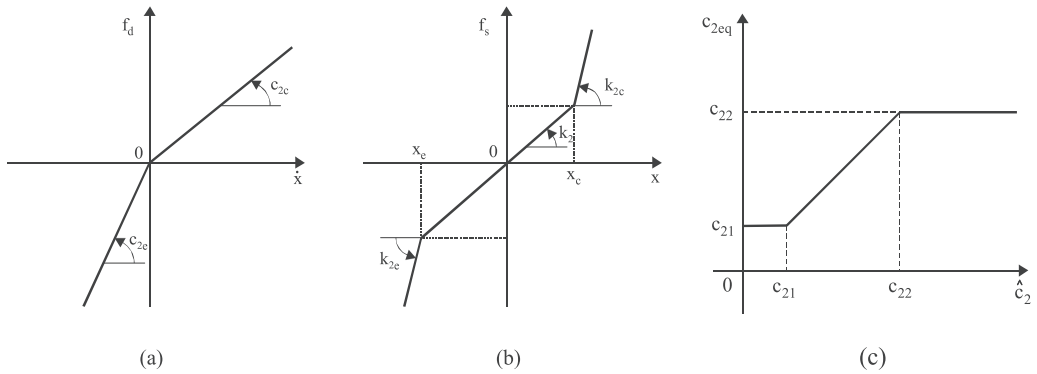


Figure 2. (a) Force characteristics of suspension damper. (b) Restoring force of suspension spring. (c) Equivalent suspension damping coefficient of sky-hook model.

The main difference between the model shown in Figure 1(b) and that shown in Figure 1(a) is that the former obeys a commonly employed passive control strategy, where the value of the suspension damping coefficient $c_2$ switches between two distinct values. More specifically, for this model the damping force developed between the car body and the wheel has the form

$$f_d(\dot{x}) = \begin{cases} c_{2c}\dot{x}, & \text{if } \dot{x} \geq 0 \\ c_{2e}\dot{x}, & \text{if } \dot{x} < 0 \end{cases} \tag{2}$$

where $\dot{x} = \dot{x}_2 - \dot{x}_1$. This means that the suspension damping coefficient depends on the sign of the relative velocity between the sprung mass and the unsprung mass, as depicted in Figure 2(a). Namely, it takes a different value in compression than in extension (e.g. Wallaschek, 1990; Surace et al., 1992). In addition, the suspension spring may also possess piecewise linear characteristics. In general, the restoring force in a typical car suspension exhibits nonlinear characteristics and can be represented with sufficient accuracy by the following expression

$$f_s(x) = \begin{cases} k_{2c}x + (k_2 - k_{2c})x_c & \text{if } x > x_c \\ k_2 x & \text{if } x_e \leq x \leq x_c \\ k_{2e}x + (k_2 - k_{2e})x_e & \text{if } x < x_e \end{cases}$$

where $x = x_2 - x_1$, while $x_c$ and $x_e$ represent clearances in the suspension (see Figure 2(b)).

Finally, the mechanical model shown in Figure 1(c) is known as an ideal "sky-hook" model and presents certain advantages over the models with conventional suspension (Verros et al., 2000b). Besides the sky-hook damper, this model includes also a ground-hook damper, with damping coefficient $c_g$, which is much larger than the equivalent damping coefficient $c_1$ of the tires. In its simplest form, this model possesses linear characteristics. However, since

it is impossible to materialize this type of suspension, an appropriate control strategy has to be applied, modifying its characteristics. According to previous studies on the subject, the behavior of the sky-hook model is approached by applying the following control force

$$F_c = c_{sky}\dot{x}_2 + c_2(\dot{x}_2 - \dot{x}_1) - c_g(\dot{x}_1 - \dot{x}_g)$$

between the two masses of the system. This implies that for an active control of the vehicle a continuous monitoring of the suspension damping coefficient value, say $\hat{c}_2$, is required, based on a measurement of the quantities $\dot{x}_1$, $\dot{x}_2$, and $\dot{x}_g$, so that

$$\hat{c}_2 \equiv \frac{F_c}{\dot{x}_2 - \dot{x}_1}.$$

In practice, the most economical and easily realizable strategy is based on a semi-active control logic, obtained with a dual-switch damper. More specifically, the equivalent suspension damping coefficient is selected from the formula

$$c_{2eq} = \begin{cases} c_{21}, & \text{if } \hat{c}_2 < c_{21} \\ \hat{c}_2, & \text{if } c_{21} \le \hat{c}_2 \le c_{22} \\ c_{22}, & \text{if } \hat{c}_2 > c_{22} \end{cases} \tag{3}$$

where $c_{21}$ and $c_{22}$ are appropriately chosen damping coefficient values (see Figure 2(c)).

The dynamical systems resulting after the application of either the passive bilinear or the semi-active control strategies are strongly nonlinear, since the value of the suspension damping coefficient changes at certain points. Moreover, a strongly nonlinear effect is introduced even for the systems with linear characteristics, when the wheel is allowed to separate and lift off the ground temporarily. This phenomenon, known as wheel hop in the literature, causes drastic changes in the overall dynamic response of the vehicle (Verros and Natsiavas, 2001). In order to include this possibility in the mechanical models examined, the following kinematical variable is first introduced

$$X_1(t) = x_1(t) - x_g(t).$$

Then, if $X_1 < 0$, the wheel is not in contact with the ground, while the loss of contact is in effect during the time intervals where the contact force

$$F_w = k_1 X_1 + (c_1 + c_g)\dot{X}_1, \tag{4}$$

which is developed between the wheel and the ground, is equal to zero (Leine et al., 2000). Finally, the corresponding modification in the equations of motion is that during the wheel hop phases the terms $k_1$, $c_1$ and the forcing function $\underline{f}(t)$ are set equal to zero.

## 3. RESPONSE CHARACTERISTICS UNDER RANDOM ROAD PROFILES

In general, a typical road is characterized by the existence of large isolated irregularities, such as potholes or bumps, which are superposed to smaller but continuously distributed profile irregularities. For the purposes of the present study, only the latter type of road irregularities are considered. Namely, this section deals with the estimation of the second-order moment response characteristics of the vehicle models presented in the previous section, traveling over road profiles that are characterized by random fields. These random fields are real-valued, zero mean, stationary, and Gaussian. Therefore, for their complete statistical description it is sufficient to specify their second-order moment. Here, this requirement is fulfilled by assuming that the road irregularities possess a known single-sided power spectral density, say $S_g(\Omega)$, where $\Omega = 2\pi/\lambda$ is a spatial frequency, corresponding to a harmonic irregularity with wavelength $\lambda$. According to many previous investigations on the subject (e.g. Dodds and Robson, 1973), the geometrical profile of typical roads fits sufficiently accurately the following simple analytical form

$$S_g(\Omega) = A_g \Omega^{-n}, \tag{5}$$

which is represented by a line in a log–log scale. In this way, the amplitude ratio of the roughness between two different road profiles is proportional to the square root ratio of the respective $A_g$ values. Moreover, it is frequently quite accurate and analytically convenient to select the value $n = 2$ for the exponent in equation (5), which in turn implies that the road slope exhibits characteristics similar to a white noise signal.

Qualitatively, a large value of the exponent $n$ in equation (5) accentuates the roughness at the longer wavelengths, while it suppresses the roughness at the shorter wavelengths. For this reason, it is commonly accepted that the spectra corresponding to the geometrical profile of typical roads can be approximated by the following, more involved function

$$S_g(\Omega) = \begin{cases} S_g(\Omega_0)(\Omega/\Omega_0)^{-n_1}, & \text{if } \Omega \le \Omega_0 \\ S_g(\Omega_0)(\Omega/\Omega_0)^{-n_2}, & \text{if } \Omega \ge \Omega_0 \end{cases} \tag{6}$$

where $\Omega_0 = 1/2\pi$ is a reference spatial frequency. Moreover, the value $S_g(\Omega_0)$ provides a measure for the roughness of the road. Here, the exponents are chosen so that $n_1 \neq n_2$ and the resulting spectrum exhibits a slope discontinuity at $\Omega = \Omega_0$ in a log–log scale. Finally, since the value of $S_g(\Omega)$ approaches infinity as $\Omega \to 0$, the road spectrum is filtered by a high pass filter.

For the special case of vehicle models with linear properties, knowledge of the road profile spectral density and the vehicle velocity permits evaluation of the spectral density of the stationary vehicle response through the well-known formula (Lutes and Sarkani, 1997)

$$S_{xx}(\omega) = H(\omega) S_{gg}(\omega) H^{\mathrm{T}^*}(\omega).$$

In the previous equation, $\omega = \Omega v_0$ is the temporal frequency, $S_{xx}(\omega)$ and $S_{gg}(\omega)$ represent the spectral density matrices of the response and the forcing, respectively, $H(\omega)$ is the matrix including the frequency response functions of the system, while the superscripts T and $*$ denote transposition and conjugation, respectively (e.g. Roberts and Spanos, 1990). The second moment characteristics of various response quantities are readily obtained by the integral over $\omega$ of the power spectral density function corresponding to these responses. However, all the vehicle models presented in the previous section, with the exception of the linear models with no wheel hop, possess equations of motion involving strong nonlinearities. In such cases, the frequency domain analysis is no longer valid and an analytical formulation for the second moment response characteristics is not available. For such cases, the probabilistic characteristics of the response are evaluated using Monte Carlo simulations, in conjunction with appropriate integration methodologies developed earlier for piecewise linear systems (e.g. Natsiavas, 1993; Verros et al., 2000b).

In particular, for nonlinear vehicle models, samples of the road profile are generated using the spectral representation method (Shinozuka, 1972; Shinozuka and Deodatis, 1991). More specifically, if the vehicle is assumed to travel with a constant horizontal speed $v_0$ over a given road, the forcing resulting from the road irregularities can be simulated by the following series

$$x_g(t) = \sum_{n=1}^{N} s_n \sin(n\omega_0 t + \varphi_n). \tag{7}$$

In the previous equation, the amplitudes $s_n = \sqrt{2S_g(n\Delta\Omega)\Delta\Omega}$ of the excitation harmonics are evaluated from the road spectra selected, where $\Delta\Omega = 2\pi/L$ and $L$ is the length of the road segment considered. In addition, the value of the fundamental temporal frequency $\omega_0$ is determined from

$$\omega_0 = \frac{2\pi}{L} v_0,$$

while the phases $\varphi_n$ are treated as random variables, following a uniform distribution in the interval $[0,\ 2\pi)$. Then, the response of the vehicle to each sample road profile is computed by integrating the equations of motion. Finally, the second moment characteristics of the response are estimated using the sample responses. A few hundred samples are usually sufficient to obtain suitable estimates of the second moments of the response.

The aforementioned method of selecting the base excitation history requires knowledge of the power spectral density of the road profile examined and the horizontal component of the vehicle velocity. Figure 3(a) shows the spectra of two sets of roads, which are used as examples in the numerical calculations performed in the fifth section. More specifically, the lower curve represents good-quality roads (with $n_1 = 2$, $n_2 = 1.5$ and $S_g(\Omega_0) = 16 \times 10^{-6}$ m$^2$ cycle$^{-1}$ m$^{-1}$), while the upper curve represents bad-quality roads (with $S_g(\Omega_0) = 256 \times 10^{-6}$ m$^2$ cycle$^{-1}$ m$^{-1}$), according to ISO 2631 standards. Figure 3(b) shows the specific forms of two typical road profiles, one belonging to the good-quality group and the other to the bad-quality group.

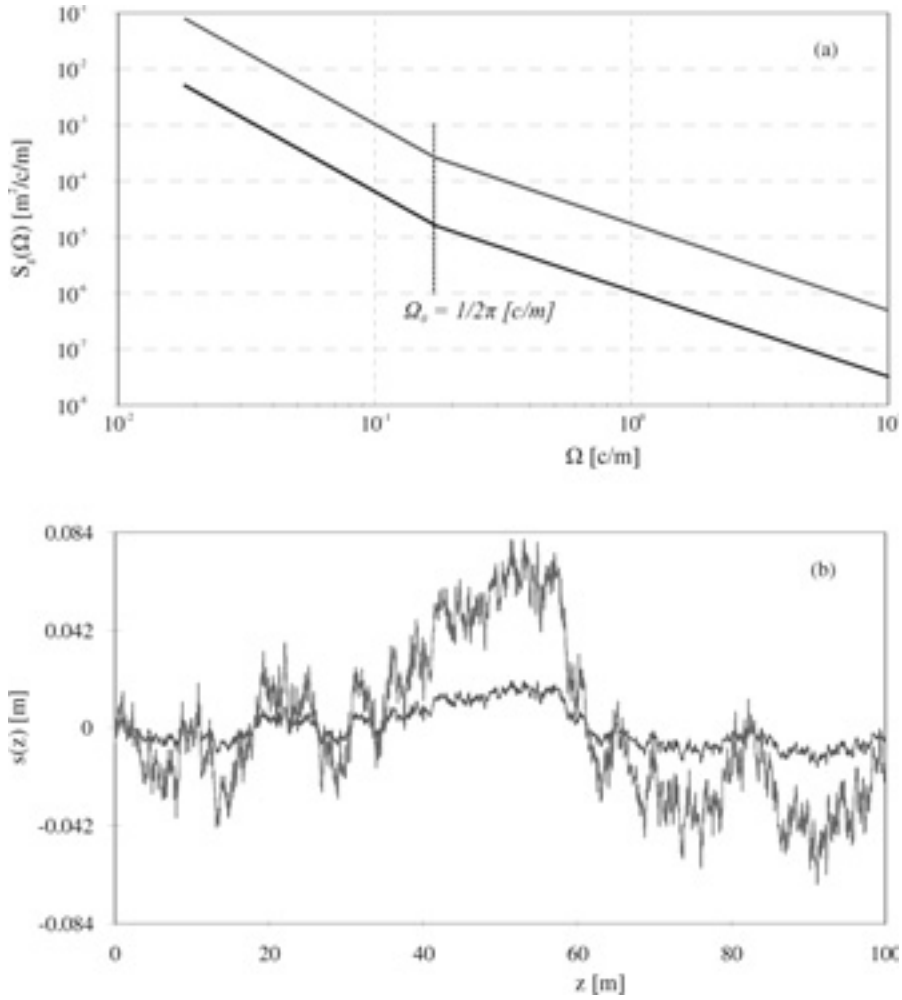


Figure 3. (a) Response spectra of typical roads and (b) profiles of a good-quality road and a poor-quality road.

## 4. VEHICLE PERFORMANCE INDEX

In this section, a systematic methodology is presented for optimizing the suspension characteristics with respect to ride comfort, vehicle handling, and working space of the suspension, taking into account the random nature of the variability of the road profiles. The methodology leads to an optimal selection of the suspension damping and stiffness parameters in ground vehicles subjected to random road excitation. The characteristics of the suspension are selected to optimize the vehicle performance over a range of vehicle velocities and under different road profiles.

Typically, evaluation of the vehicle performance is based on examination of three response quantities, within a prespecified frequency range (Gillespie, 1992); that is, the max-

imum absolute acceleration $\ddot{x}_2$ of the passengers, the distance $x_2 - x_1$ between the wheel subsystem and the car body and the force $F_w$ developed between the wheel and the ground, as defined by equation (4). Therefore, taking into account the random nature of the excitation applied, the performance index is identified by the following normalized expected value

$$J(\underline{\theta}) = w_1 J_1(\underline{\theta}) + w_2 J_2(\underline{\theta}) + w_3 J_3(\underline{\theta}), \tag{8}$$

with

$$\begin{aligned} J_1(\underline{\theta}) &= \frac{1}{(m_2 g)^2} E\left[\frac{1}{T}\int_0^T \{m_2 \ddot{x}_2(t;\underline{\theta})\}^2 \,\mathrm{d}t\right], \\ J_2(\underline{\theta}) &= \frac{1}{(m_2 g)^2} E\left[\frac{1}{T}\int_0^T \{k_2(x_2(t;\underline{\theta}) - x_1(t;\underline{\theta}))\}^2 \,\mathrm{d}t\right] \end{aligned}$$

and

$$J_3(\underline{\theta}) = \frac{1}{(m_2 g)^2} E\left[\frac{1}{T}\int_0^T F_w^2(t;\underline{\theta})\mathrm{d}t\right].$$

The constants $w_1$, $w_2$, and $w_3$ denote appropriately chosen weighting coefficients, which indicate the contribution of the individual performances on ride comfort, working space of the suspension and vehicle handling on the total performance, respectively. Finally, $T = L/v_0$ is the temporal measurement period, while the vector $\underline{\theta}$ includes the set of the system technical parameters to be optimized.

The optimization (minimization) of the performance index in equation (8) requires repeated computations of the second moments of the response quantities appearing in equation (8) for different values of the parameter set $\underline{\theta}$. For linear systems and stationary response, the second moments of the responses can be obtained using the analytical formulation for the spectral density function of the response. For the nonlinear vehicle models, the estimation is done using Monte Carlo simulations as described in the previous section. More details on the numerical implementation of this optimization process are presented in the following section.

## 5. NUMERICAL RESULTS

The analysis presented in the previous sections can be applied to any multiple-degrees-of-freedom vehicle model. In this section, typical numerical results are presented for the example two-degrees-of-freedom models shown in Figure 1. First, quarter-car models involving linear characteristics are examined. Then, car models with piecewise linear damping and stiffness are considered. Finally, results obtained for car models with semi-active suspensions are also presented. An effort is made to select the optimum values of the suspension damping and stiffness parameters for a range of vehicle velocity values, by considering the effects of road quality and accounting for the possibility of wheel hop.

### *5.1. Results for Car Models with Linear Suspension Dampers*

For the linear models examined, the nominal parameter values are selected to be the following: $m_1 = 60$ kg, $m_2 = 375$ kg, $k_1 = 200$ kN m$^{-1}$, $k_2 = 15$ kN m$^{-1}$, $c_1 = 7$ Ns m$^{-1}$ and $c_2 = 1425$ Ns m$^{-1}$. Moreover, a good-quality road with length $L = 100$ m is considered, according to the process presented in Section 3, while the vehicle speed range is chosen to extend from 40 to 180 km h$^{-1}$. The lower part of this velocity spectrum is more appropriate to conditions of driving on a town street or on a relatively poor-quality road, while the higher part covers cases of fast driving on a high-quality freeway.

First, Figure 4(a) shows the optimum value obtained for the suspension damping coefficient $c_2$, while Figure 4(b) presents the optimum value of the stiffness coefficient $k_2$ for the combination $w_1 = w_2 = w_3 = 1/3$, as a function of the vehicle speed $v_0$. The thick curves on these diagrams were determined by applying the optimization process to the parameter set $\underline{\theta} = (c_2 \;\; k_2)^{\mathrm{T}}$, while the thin lines were determined by considering the corresponding parameter alone. Clearly, the thin and thick curves exhibit the same qualitative behavior throughout the velocity speed spectrum considered. For the damping coefficient, the larger quantitative deviations are observed in the range of the higher speeds. Since the optimum values of both parameters depend on the vehicle velocity, special care should be taken when a relatively wide range of velocities needs to be considered. For instance, in view of the existence of multiple terms in the objective function, a multi-objective programming procedure may be more appropriate in such cases (Matusov, 1995; Gobbi and Mastinu, 2001).

In an effort to illustrate the effect of the weighting coefficients in the composite performance index defined by equation (8), Figure 5 presents results obtained by applying optimization with respect to the parameter set $\underline{\theta} = (c_2 \;\; k_2)^{\mathrm{T}}$ and different combinations of $w_1$, $w_2$, and $w_3$. Clearly, choosing different weighting of the terms in the performance index leads to different optimum values for the suspension parameters. However, in all cases examined, the results for both $c_2$ and $k_2$ look qualitatively similar to those presented in Figure 4.

Before proceeding further, it is useful to provide some explanation for the optimization results presented so far. This is accomplished by examining the dynamics of the system considered. In particular, Figure 6 presents the spectra of the quantities $\ddot{x}_2$, $x_2 - x_1$, $\dot{x}_2 - \dot{x}_1$, and $F_w$, obtained under harmonic road excitation with frequency $\omega$ and several values of the suspension damping coefficient $c_2$. First, the results of Figure 6(a) demonstrate that an increase in $c_2$ causes a reduction in the amplitude of the vehicle body acceleration $\ddot{x}_2$ only in the vicinity of the two resonances, while it may have a diverse effect away from the resonances. On the other hand, the results shown in Figures 6(b) and (c) illustrate that an increase in $c_2$ causes always a reduction in the amplitude of both the relative displacement $x_2 - x_1$ and the relative velocity $\dot{x}_2 - \dot{x}_1$. In fact, for sufficiently large values of $c_2$, the maximum amplitude of both of these quantities moves to the characteristic frequency $\sqrt{k_2/(m_1 + m_2)}$, as expected. Finally, the results included in Figure 6(d) indicate that the effect of increasing $c_2$ is beneficial in decreasing the value of the tire force $F_w$ in the vicinity of the two resonances, as well as in the high forcing frequency range. However, the tire force values are accentuated between the two resonances by increasing $c_2$. In view of the linearity of the system examined and the validity of the superposition principle, the trends in the dynamics observed in the diagrams of Figure 6 can lead to a better understanding of the optimization results presented in Figures 4 and 5.

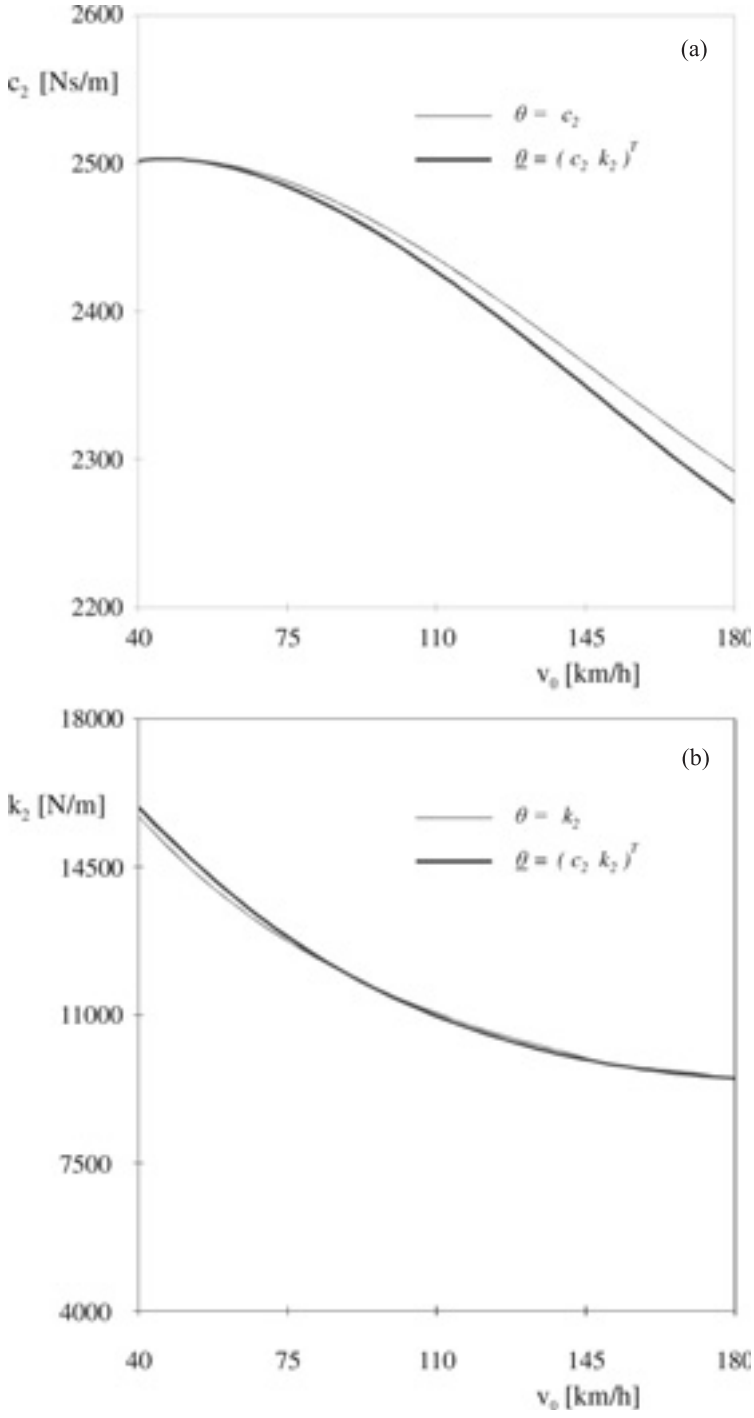


Figure 4. Optimum values for (a) the suspension damping coefficient $c_2$ and (b) the suspension stiffness coefficient $k_2$, for a quarter-car model with linear suspension damper.

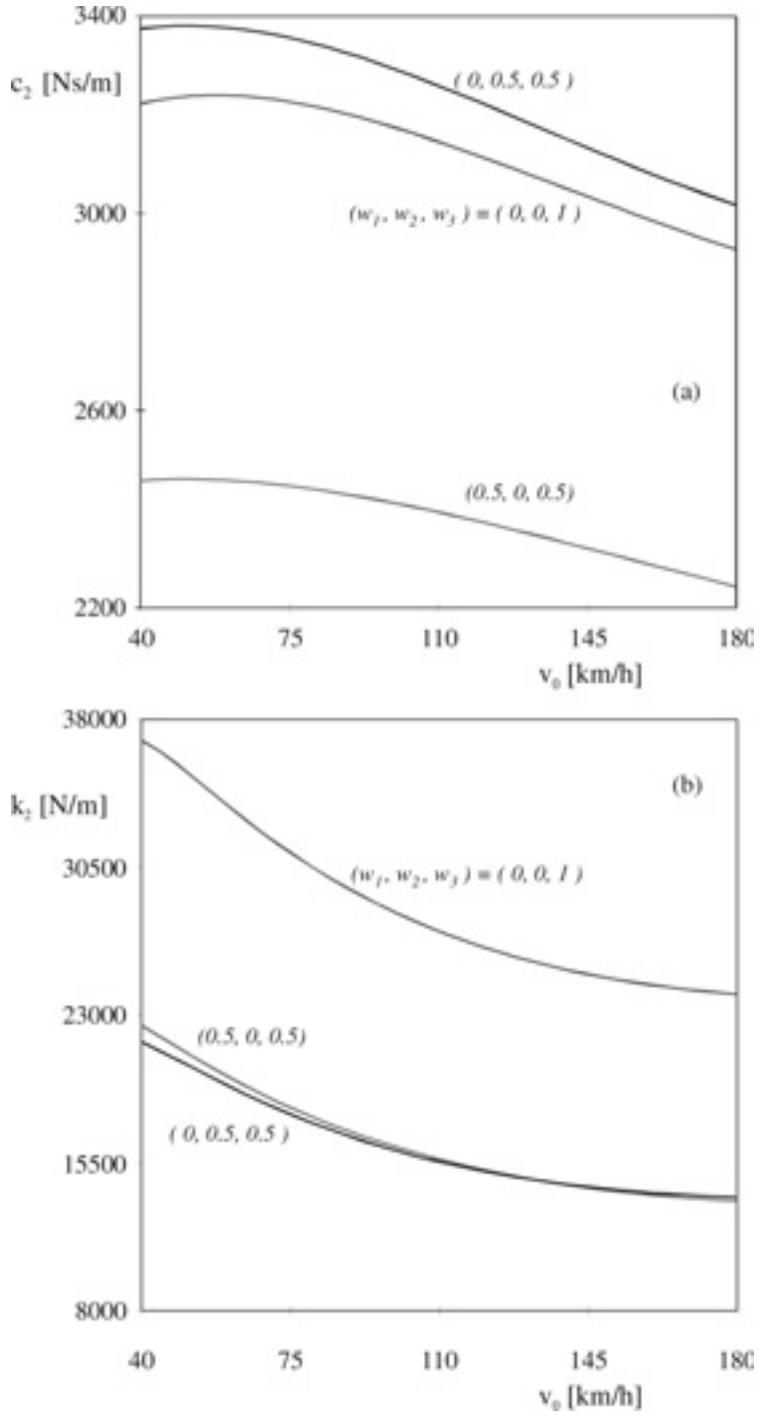


Figure 5. Optimum values for (a) the suspension damping coefficient $c_2$ and (b) the suspension stiffness coefficient $k_2$, for different values of the weighting coefficients.

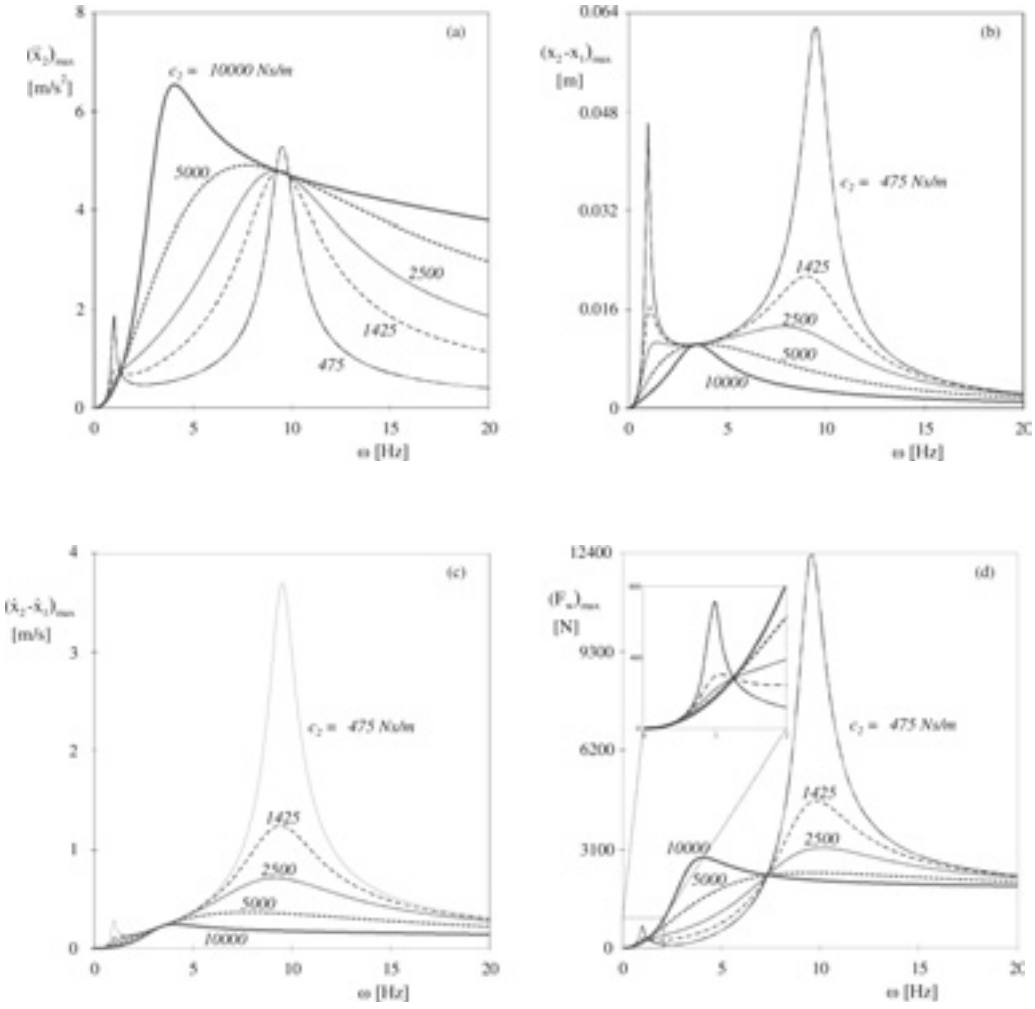


Figure 6. Response spectra of linear car models for (a) the vehicle body acceleration $\ddot{x}_2$, (b) the relative displacement $x_2 - x_1$, (c) the relative velocity $\dot{x}_2 - \dot{x}_1$, and (d) the tire force $F_w$.

The picture is clarified further by the results presented in the following set of diagrams. More specifically, Figures 7(a)–(c) illustrate the dependence of the functions $J_n$ ($n = 1, 2, 3$) included in the performance index (8) on the suspension damping coefficient, for the two extreme values of the velocity spectrum considered. First, direct comparison indicates that there is a shift in the minimum value of each of these functions as $v_0$ varies. This shift is expected since an increase in the value of $v_0$ causes an increase in the frequencies of the road excitation signal. On the other hand, Figure 7(d) depicts the history of the tire force $F_w$, obtained on a real road at $v_0 = 180$ km h$^{-1}$, for three selected values of the suspension damping coefficient $c_2$. Similar characteristics are also observed to occur in the history of the response quantities $\ddot{x}_2$ and $x_2 - x_1$, and demonstrate that the minimum value of each function $J_n$ is reached at an intermediate value of $c_2$, which is different for each $J_n$. This

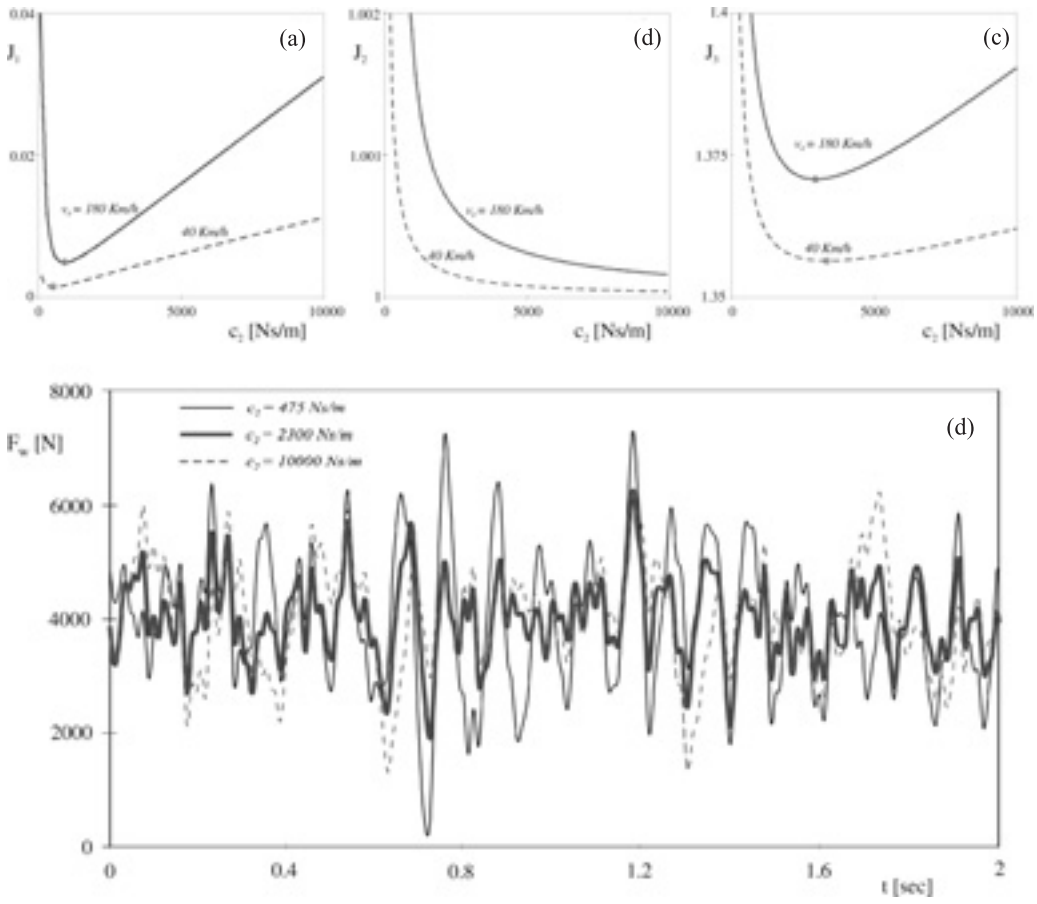


Figure 7. (a)–(c) Dependence of the functions $J_n$ ($n = 1, 2, 3$) on the suspension damping coefficient $c_2$, for the two extreme values of the vehicle speed $v_0$. (d) History of tire force $F_w$, obtained at $v_0 = 180$ km h$^{-1}$ for three selected values of the suspension damping coefficient $c_2$.

observation can be justified by the different effect the suspension damping level has on the response quantities included in $J_n$ before and after the resonance frequencies of the system examined, as illustrated by the results of Figure 6. Finally, the results shown in Figures 4(b) and 5(b) can also be justified in a similar manner, by examining the effect of the suspension stiffness coefficient $k_2$ on the system dynamics.

In all the example cases investigated so far, no wheel hop phenomena were observed to occur, due mainly to the good quality of the road profiles selected. The following set of results was obtained in an effort to investigate effects of the road quality and wheel hop. More specifically, the results of Figure 8 were obtained after selecting a poor-quality road, for $\underline{\theta} = (c_2 \;\; k_2)^{\mathrm{T}}$ and $w_1 = w_2 = w_3 = 1/3$. The continuous thick curves were obtained for car models where no wheel hop is allowed to take place, while the thin curves refer to models including the wheel hop possibility. In the former case, qualitatively similar trends as before are observed once again for the optimum value of both the suspension damping and

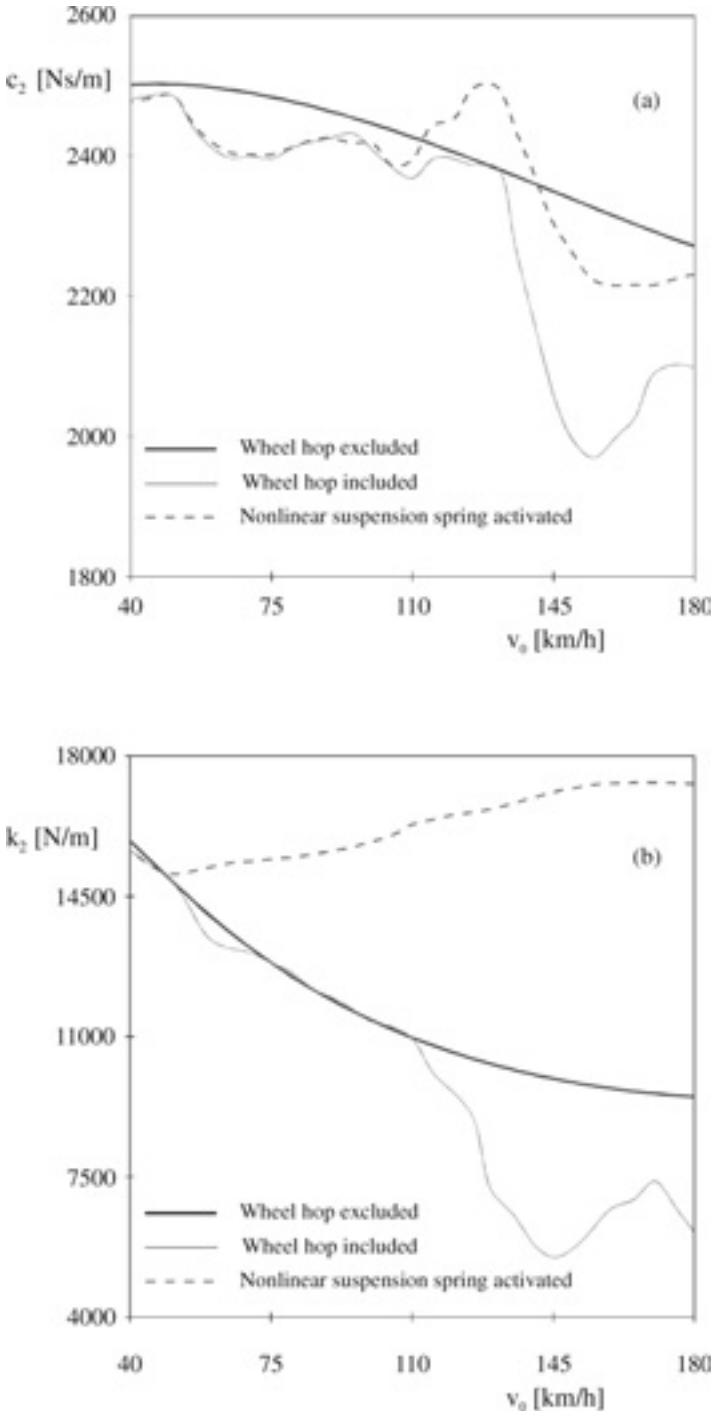


Figure 8. Optimum values for (a) the suspension damping coefficient $c_2$ and (b) the suspension stiffness coefficient $k_2$, of a quarter-car model with wheel hop and nonlinear spring.

stiffness coefficient, throughout the velocity interval considered. However, the performance index accepts much higher values for the poor-quality road. Moreover, the data obtained from the models allowing wheel hop present significant differences, especially in the higher range of the velocity spectrum.

The optimization results obtained originally for the poor-quality road excitation were based on the assumption that the suspension spring remains always within its linear range. However, inspection of the response histories captured indicated that the relative displacement of the wheel with respect to the car body may become temporarily so excessive that the upper part of the trilinear spring shown in Figure 2(b) is activated. Therefore, in order to complete the picture, the results represented by the dashed lines in Figure 8 were determined by taking into account the exact characteristics of the suspension spring, as shown in Figure 2(a), with $x_{cp} = 0.28$ m and $k_{2p} = 700$ kN m$^{-1}$. For the suspension damping coefficient, the effect of including the piecewise linear nature of the suspension spring is more important for relatively high car velocities. However, the value of the stiffness coefficient $k_2$ is significantly affected almost throughout the velocity range considered. These results demonstrate the important effects of the suspension nonlinearities on the design, which are due to the complex dynamics they induce.

### *5.2. Results for Car Models with Bilinear Suspension Dampers*

In this subsection, we present results obtained for car models with a passive bilinear suspension damper. The default values of the suspension damping coefficient employed in the subsequent calculations are $c_{2c} = 475$ Ns m$^{-1}$ and $c_{2e} = 1425$ Ns m$^{-1}$, respectively. Moreover, in all cases examined a good-quality road was selected, while the values of the weighting coefficients were chosen as $w_1 = w_3 = 0.5$ and $w_2 = 0$.

First, the continuous thick lines in Figure 9 were determined by optimizing with respect to the parameter set $\underline{\theta} = (c_{2c} \;\; c_{2e})^{\mathrm{T}}$, while the thin lines were determined by considering the corresponding damping parameter alone. Moreover, the dashed lines represent data obtained for $\underline{\theta} = (k_2 \;\; c_{2c} \;\; c_{2e})^{\mathrm{T}}$. Here, the deviations appearing when a single or both the damping parameters are considered are more visible. Also, the optimum value of the suspension damping coefficient in compression presents qualitatively similar trends with those observed before for the models with linear suspension damper. However, the suspension damping coefficient in extension seems to follow an opposite trend. Finally, the effects from including the suspension stiffness in the set of the optimization parameters are more pronounced for the higher car velocity values.

As a consequence of the opposite trends observed in the dependence of the suspension damping coefficients on the car velocity, the value of the ratio $c_{2e}/c_{2c}$ accepts very different values within the velocity range considered, as shown in Figure 9(c). In particular, the ratio of the damping coefficient in extension to the damping coefficient in compression starts from a value of less than unity in the lower velocity range, but it quickly passes over one and climbs gradually up to a value of 3.7 at the higher velocity values. This result is in agreement with an empirical rule of thumb appearing in the relevant literature, where it is claimed that the optimum damping effects are realized when the damping coefficient in rebound (extension) must be larger than the damping coefficient in jounce (compression). In fact, it is specifically suggested that the optimum value of this ratio must be equal to three

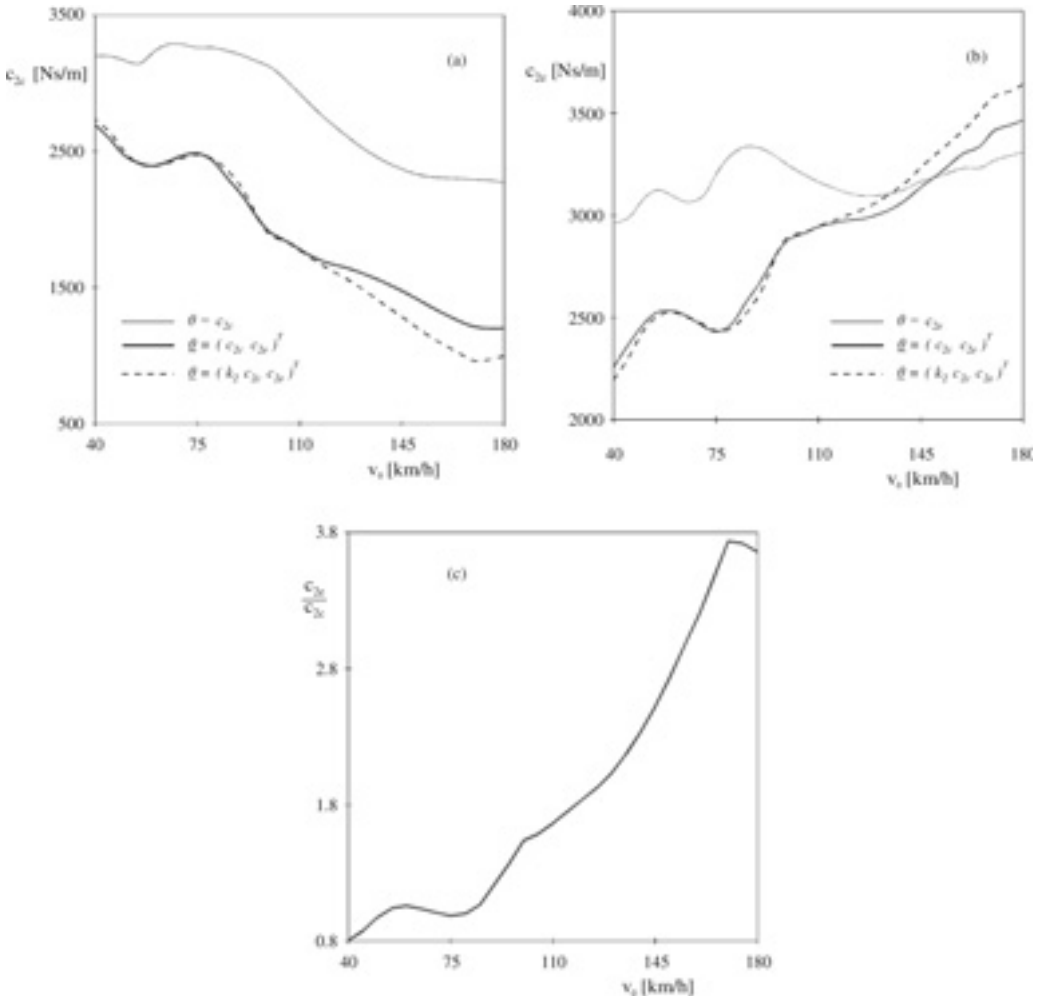


Figure 9. Optimum values for the suspension damping coefficient in (a) compression and (b) extension, for a quarter-car model with bilinear suspension damper. (c) Dependence of the suspension damping coefficient ratio $c_{2e}/c_{2c}$ on the horizontal vehicle speed $v_0$.

(Gillespie, 1992). However, as the numerical results indicate, the optimum value of this ratio is a strong function of the car velocity. Moreover, it is also dependent on other factors, such as the road quality, the weighting factors in the performance index, and the specific technical characteristics of the vehicle considered.

In order to explain why the dependence of the damping parameter $c_{2e}$ on the speed $v_0$ exhibits an opposite trend to that of $c_{2c}$, the attention was shifted to the dynamics of the system examined, once again. First, Figure 10(a) depicts the maximum and the minimum values of the car body acceleration $\ddot{x}_2$, obtained under harmonic road excitation for $c_{2c} = 475$ Ns m$^{-1}$ and three selected values of $c_{2e}$. Likewise, Figure 10(b) depicts similar spectra, obtained for $c_{2e} = 1425$ Ns m$^{-1}$ and selected values of $c_{2c}$. These results were obtained

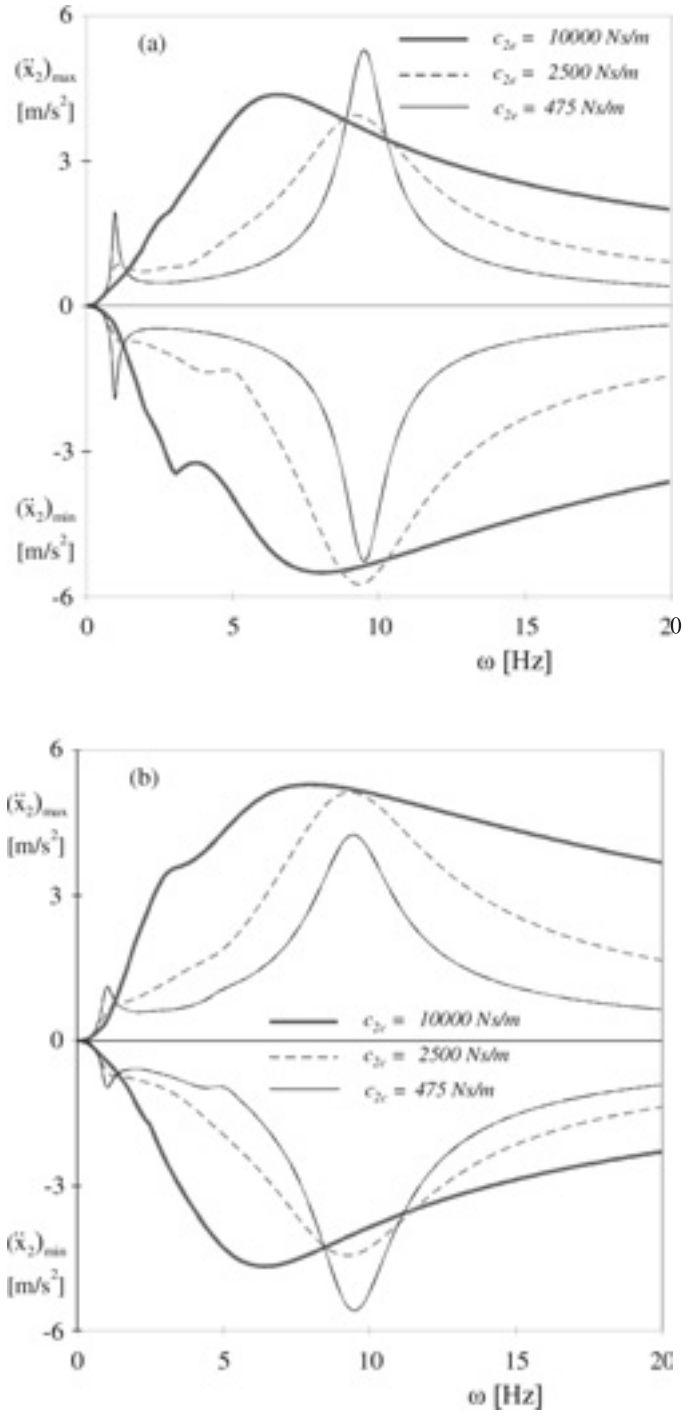


Figure 10. Response spectra (maximum and minimum values) of the vehicle body acceleration $\ddot{x}_2$ for quarter-car models with dual-rate dampers: (a) $c_{2c} = 475$ Ns m$^{-1}$ and several values of $c_{2e}$; (b) $c_{2e} = 1425$ Ns m$^{-1}$ and several values of $c_{2c}$.

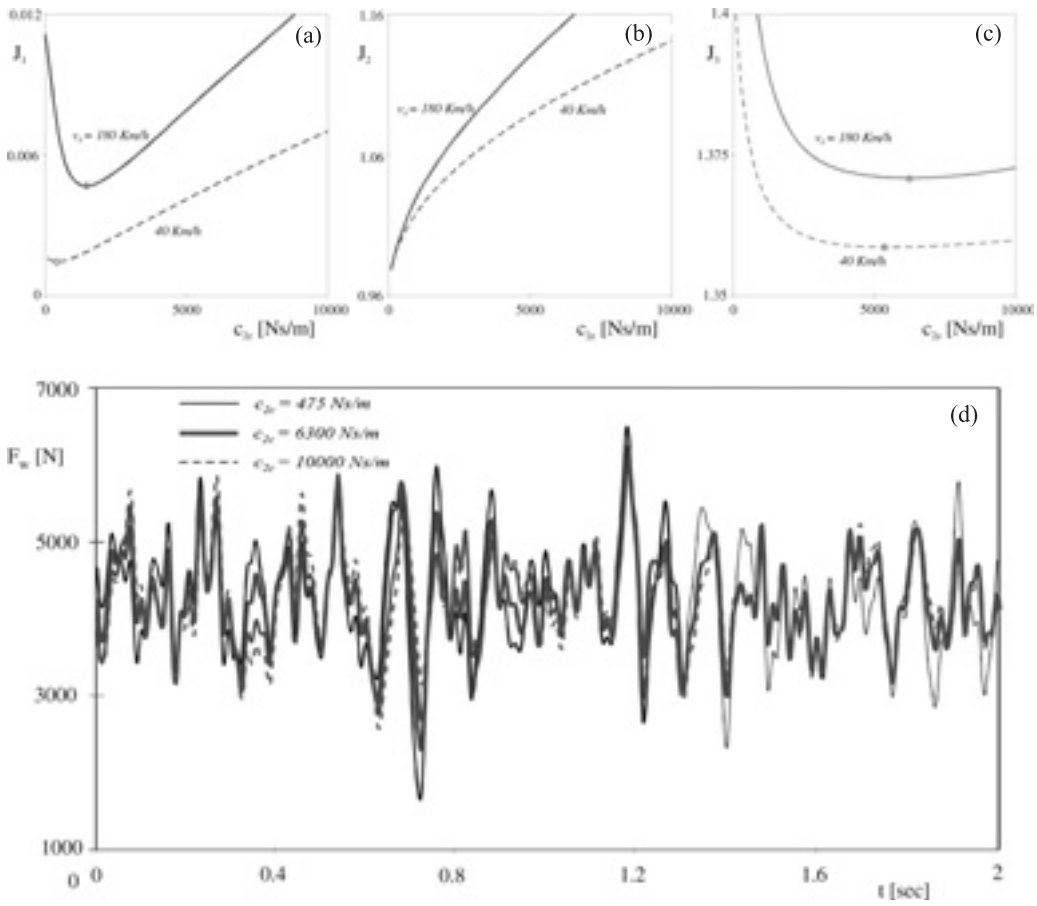


Figure 11. (a)–(c) Dependence of the functions $J_n$ $(n = 1, 2, 3)$ on the suspension damping coefficient $c_{2e}$, for the two extreme values of the car speed $v_0$. (d) History of tire force $F_w$, obtained at $v_0 = 180$ km h$^{-1}$ for three selected values of the suspension damping coefficient $c_{2e}$.

by applying special techniques developed earlier for piecewise linear oscillators (Natsiavas, 1993). Similar results were also obtained for the other response quantities included in the cost function. What is most interesting in all these results is that the difference in the damping coefficients $c_{2c}$ and $c_{2e}$ is responsible for the appearance of an asymmetry in all the response quantities. In particular, the spectra obtained for a specific combination, say $(c_{2c}, c_{2e}) = (\widehat{c}_1, \widehat{c}_2)$, turn out to be mirror images (with respect to the forcing frequency axis) of the spectra obtained for $(c_{2c}, c_{2e}) = (\widehat{c}_2, \widehat{c}_1)$. This asymmetry in the response is related to some important changes in the dependence of the three functions $J_n$ of the performance index (8) on the suspension damping coefficients $c_{2c}$ and $c_{2e}$, as is demonstrated with the following set of diagrams.

Figures 11(a)–(c) exhibit the dependence of the three functions $J_n$ on the suspension damping coefficient $c_{2e}$, for the two extreme values of the velocity spectrum considered. Here, there are two important points to note, related to the two dominant functions $J_2$ and $J_3$.

First, an increase in $v_0$ causes a shift in the minimum value of $J_3$ to higher values of $c_{2e}$. This is in contrast to what happens in the dependence of $J_3$ on $c_{2c}$ (which was found to be similar to that shown in Figure 7(c)) and explains the difference observed in Figures 9(a) and (b). This point is reinforced further by the results shown in Figure 11(d), which depicts the history of the tire force $F_w$, obtained on a real road at $v_0 = 180$ km h$^{-1}$, for three selected values of the suspension damping coefficient $c_{2e}$. On the other hand, the monotonic dependence of $J_2$ on $c_{2e}$, shown in Figure 11(b), explains why the computations may sometimes lead to an optimum value which coincides with one of the extreme damping values. For instance, this is the basic reason for selecting $w_2 = 0$ in the present calculations. Inclusion of a sufficiently large value of the weighting coefficient $w_2$ led to an optimum damping value coefficient $c_{2e}$ equal to zero.

Finally, the results obtained for the optimum values of the suspension stiffness coefficient of quarter-car models with bilinear suspension damping are more interesting. To demonstrate this, the continuous thin curve of Figure 12(a) was determined for the same example, by optimizing with respect to parameter $k_2$ alone, while the dashed line represents data evaluated for $\underline{\theta} = (k_2 \;\; c_{2c} \;\; c_{2e})^{\mathrm{T}}$. As a first observation, the continuous curve appears in a quite different form than that presented in Figures 4(b) and 5(b) for the linear system, reflecting a different action of the suspension stiffness parameter. Moreover, a distinct feature of the present case is that the curve indicating the dependence of $k_2$ on the car velocity exhibits sudden jumps at certain velocity values.

This seemingly peculiar behavior is justified by the results of Figure 12(b), showing the dependence of the performance index on $k_2$, for several different values of the velocity speed $v_0$ around one of the jumps. The diagrams shown indicate the existence of multiple local minima of the performance index, for the velocity range considered. The global and a local minimum observed at around $k_2 = 10$ and 25 kN m$^{-1}$ for $v_0 = 82$ km h$^{-1}$ become local and global, respectively, for $v_0 = 80$ km h$^{-1}$. This gives rise to the discontinuity in the optimal value of $k_2$ as a function of the vehicle velocity, observed at about $v_0 = 81$ km h$^{-1}$ in Figure 12(a). It should be noted that the optimization calculations may accidentally be trapped into a local minimum, depending on the initial estimate. To avoid this situation in the cases examined, the optimum value obtained was selected after comparing the corresponding values of the performance index. Finally, these jumps were eliminated when the set of optimization parameters included also the suspension damping coefficients, as demonstrated by the dashed lines in Figure 12(a).

### *5.3. Results for Sky-hook Models*

In this subsection, we present numerical results referring to quarter-car models with sky-hook characteristics. Here, the optimization process was divided into two discrete stages. In the first stage, the optimum values of the parameters of the ideal sky-hook model (Figure 1(c)), included in the vector $\underline{\theta} = (c_{sky} \;\; c_2 \;\; c_g)^{\mathrm{T}}$ were first determined for excitation arising from the group of the good-quality roads examined. The values obtained for the damping coefficients $c_2$ and $c_g$, for the combinations $w_1 = w_2 = w_3 = 1/3$ or $w_1 = w_3 = 0.5$ and $w_2 = 0$, are shown in Figure 13. Clearly, the dependence of the suspension damping coefficient $c_2$ on the vehicle speed $v_0$ appears to be similar to that observed for the linear system or to the damping coefficient in compression for the dual-rate system. Moreover, the dependence of

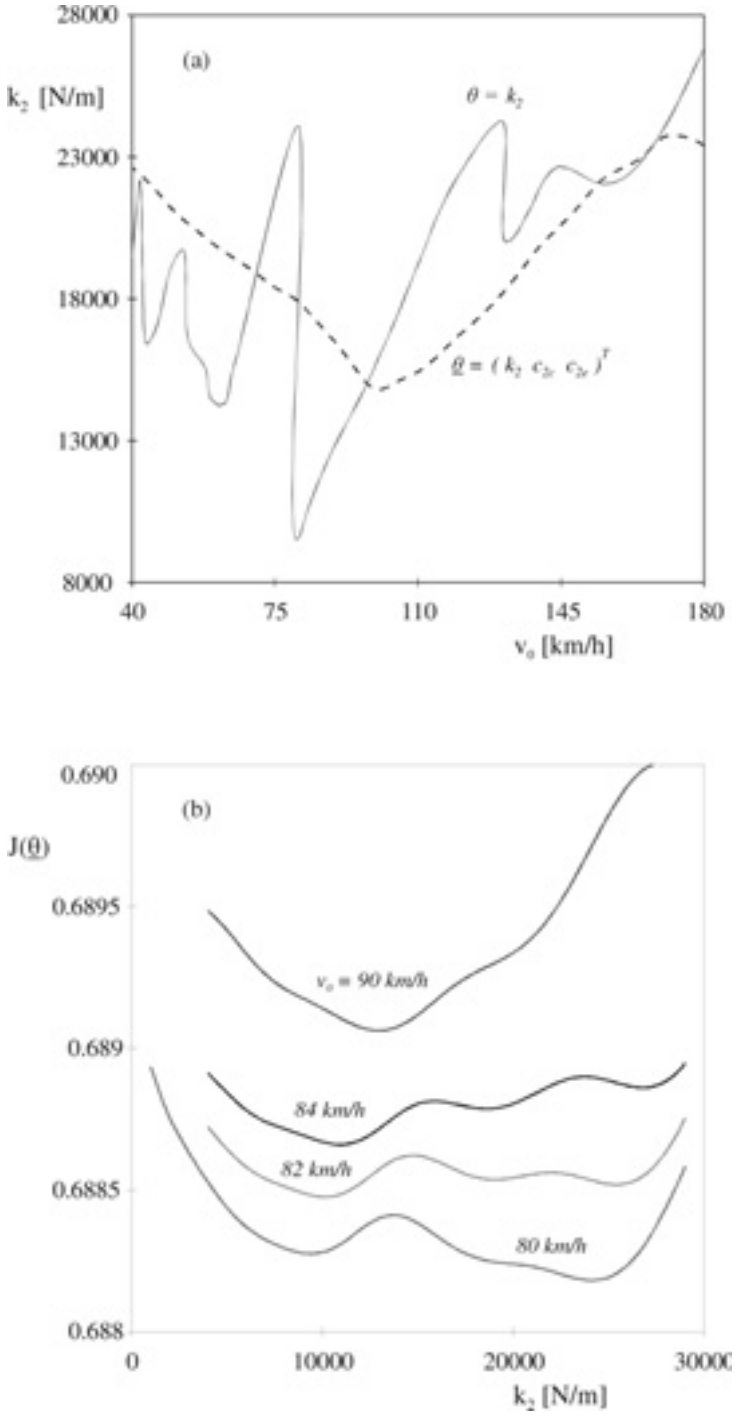


Figure 12. (a) Optimum values for the suspension stiffness coefficient $k_2$ and (b) performance index, for a quarter-car model with bilinear suspension damper.

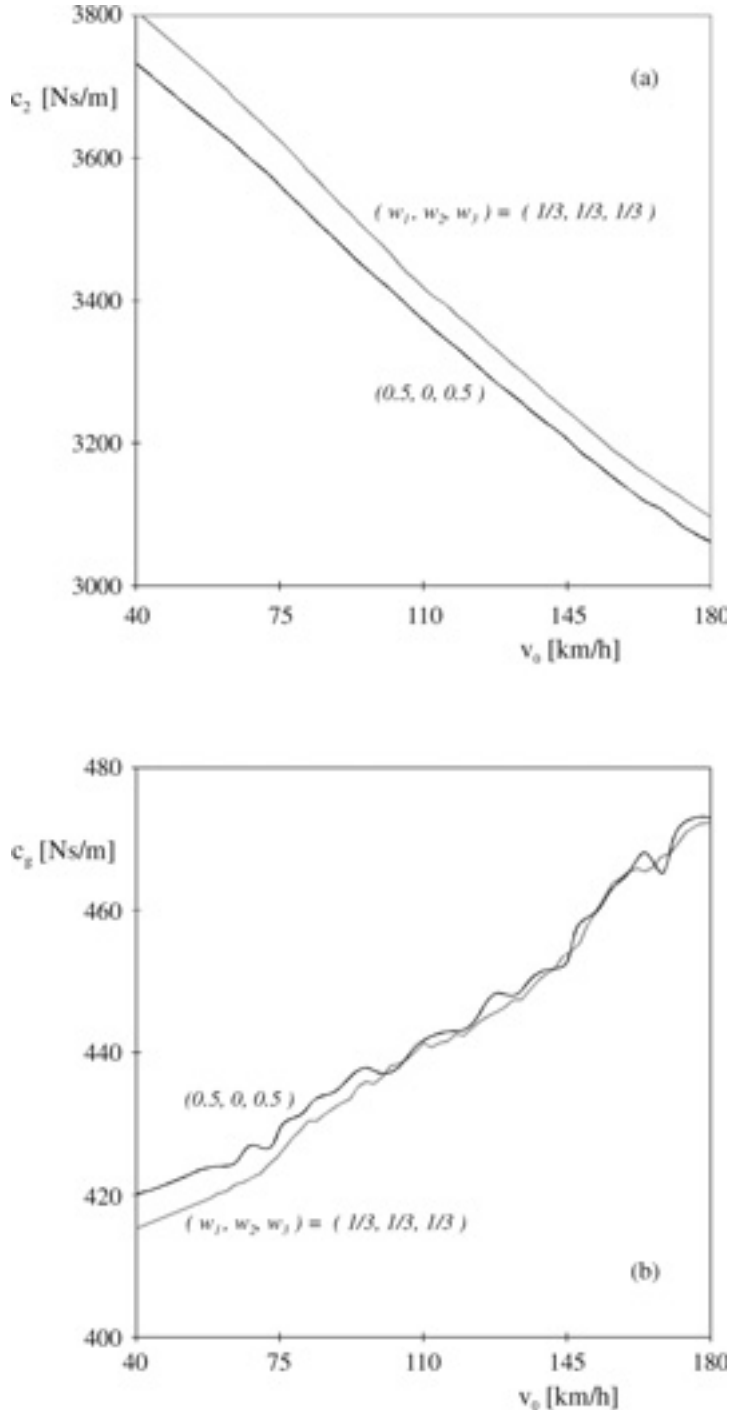


Figure 13. Optimum values for (a) the suspension damping coefficient $c_2$ and (b) the damping coefficient $c_g$, for an ideal sky-hook car model.

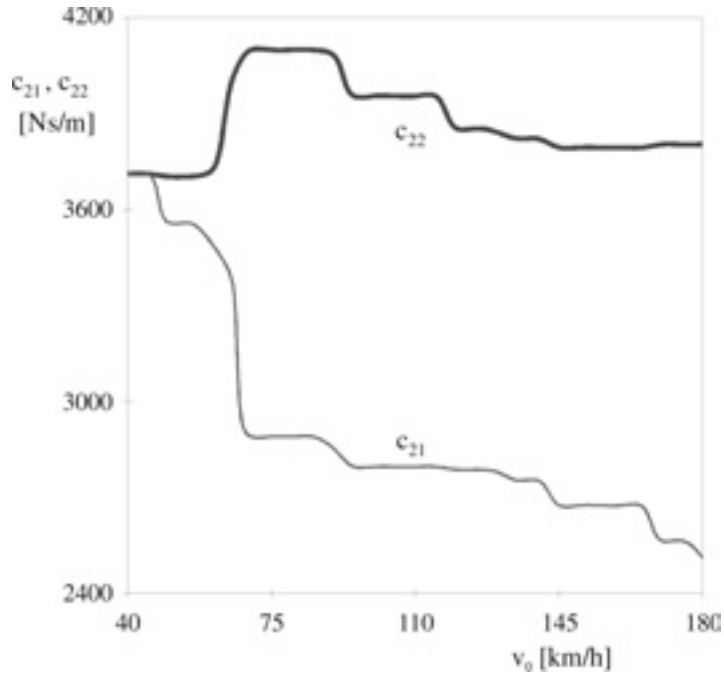


Figure 14. Optimum values for the suspension damping coefficients $c_{21}$ and $c_{22}$ of a nonlinear sky-hook car model.

the damping parameter $c_g$ on $v_0$ exhibits similar characteristics to those observed for $c_{2e}$ in the bilinear system of the previous subsection. Finally, in all cases examined the optimum value of $c_{sky}$ was found to reach a relatively high value. For this reason, its maximum allowable value was set equal to 50 kNs m$^{-1}$.

In the second stage of the optimization process, the damping parameters of the original linear sky-hook model were chosen as follows: $c_{sky} = 50$ kNs m$^{-1}$, $c_2 = 3.4$ kNs m$^{-1}$ and $c_g = 450$ Ns m$^{-1}$, taking into account the results of the first stage. Then, the optimum values for the two different suspension damping coefficients of the equivalent nonlinear model (similar to that shown in Figure 1(b)) were located by repeating the optimization process. Figure 14 presents results obtained for good-quality roads and weighting coefficients $w_1 = w_3 = 0.5$ and $w_2 = 0$. The optimum suspension damping coefficient $c_{21}$ presents a monotonically decreasing tendency to an increase in the speed value $v_0$. However, the damping coefficient $c_{22}$ exhibits a different trend in different velocity intervals.

In closing, the results of Figure 15 permit an overall critical comparison to be made between the performance of systems with linear suspension and car models with passive bilinear or semi-active shock absorbers. In particular, the thick and the nearby thin continuous curves indicate the values of the performance index obtained for a quarter-car model with a passive bilinear or a linear damper, respectively, within the car velocity range of interest. Likewise, the dashed lines represent the distribution of the performance index obtained for the approximate nonlinear sky-hook model, while the nearby continuous thin curve presents

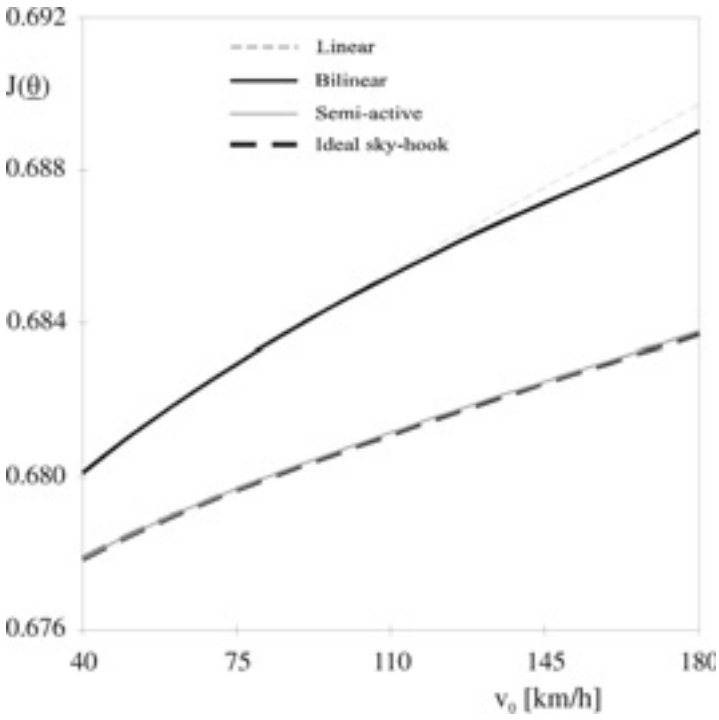


Figure 15. Comparison of performance index values for quarter-car models with a linear damper, a bilinear damper, a nonlinear sky-hook, and an ideal sky-hook damper.

similar results for the corresponding ideal sky-hook model. In all cases, the same set of good-quality roads was employed, with weighting coefficients $w_1 = w_3 = 0.5$ and $w_2 = 0$.

The results of Figure 15 demonstrate that among the different configurations examined the sky-hook models correspond to the best design possible, since they lead to the minimum value of the performance index. In fact, the difference in the values of the performance index obtained for the ideal sky-hook model (Figure 1(c)) from those obtained for the sky-hook model with variable damping is practically negligible. This provides a solid justification for the choice of the suspension damping coefficients according to the approximate eq. (3). Finally, applying the same criterion for the passively controlled model, the results of Figure 15 indicate that the performance of the car with the dual-rate damper is only slightly better than that of the car with a constant damping coefficient.

## 6. SUMMARY

In the first part of this study a systematic methodology was presented, yielding optimal values for the suspension damping and stiffness parameters of quarter-car models moving on roads with randomly varying geometrical profiles. Car models with passive linear and dual-rate suspension dampers as well as models with semi-active sky-hook damping were

examined. The control strategies applied, in conjunction with the consideration of wheel hop, led to the appearance of strong nonlinearities in the equations of motion. This in turn caused difficulties in both the integration and the optimization procedures applied, which were overcome by employing appropriate methodologies. In the second part of the work, numerical results were presented, referring mostly to optimum selection of the suspension parameters for typical quarter-car models and different combinations of the weighting factors in a suitably defined performance index. Attention was also focused on investigating effects related to the quality of the road profiles. In this case, special emphasis was placed on examining the influence of the wheel hop or the nonlinearities in the suspension spring, which were found to be activated and cause significant consequences for poor-quality roads. Some useful insight into the most important trends observed in the optimization results was also gained by examining the dynamics of the models examined. Finally, based on a critical evaluation of the information obtained from all the cases examined, it was concluded that semi-actively controlled vehicles represent better designs over car models with passive dual-rate dampers, which in turn exhibit a better performance than models with linear suspension dampers.

*Acknowledgments. This work was funded in part by the Greek Ministry of Development and the European Community Fund, through the PENED 99 program framework under grant 99ED580.*

## REFERENCES

Dixon, J. C., 1996, *Tires, Suspension and Handling*, Society of Automotive Engineers, Warrendale, PA.

Dodds, C. J. and Robson, J. D., 1973, "The description of road surface roughness," *Journal of Sound and Vibration* **31**, 175–183.

Gillespie, T. D., 1992, *Fundamentals of Vehicle Dynamics,* Society of Automotive Engineers, Warrendale, PA.

Gobbi, M. and Mastinu, G., 2001, "Analytical description and optimization of the dynamic behavior of passively suspended road vehicles," *Journal of Sound and Vibration* **245**, 457–481.

Harrison, R. F. and Hammond, J. K., 1986, "Approximate, time-domain, non-stationary analysis of stochastically excited, non-linear systems with particular reference to the motion of vehicles on rough ground," *Journal of Sound and Vibration* **105**, 361–371.

Hrovat, D., 1993, "Application of optimal control to advanced automotive suspension design," *ASME Journal of Dynamic Systems, Measurement and Control* **115**, 328–342.

Karnopp, D., Crosby, M. J., and Harwood, R. A., 1974, "Vibration control using semi-active generators," *ASME Journal of Engineering for Industry* **96**, 619–626.

Leine, R. I., Van Campen, D. H., and Van de Vrande, B. L., 2000, "Bifurcations in nonlinear discontinuous systems," *Nonlinear Dynamics* **23**, 105–164.

Lutes, L. D. and Sarkani, S., 1997, *Stochastic Analysis of Structural and Mechanical Vibrations*, Prentice-Hall, Englewood Cliffs, NJ.

Matusov, J., 1995, *Multicriteria Optimization and Engineering,* Chapman & Hall, New York.

Metallidis, P., Verros, G., Natsiavas, S., and Papadimitriou, C., 2003, "Fault detection and optimal sensor location in vehicle suspensions," *Journal of Vibration and Control* **9**, 337–359.

Natsiavas, S., 1993, "Dynamics of multiple degree of freedom oscillators with colliding components," *Journal of Sound and Vibration* **165**, 439–453.

Palkovics, L. and Venhovens, P. J. Th., 1992, "Investigation on stability and possible chaotic motions in the controlled wheel suspension system," *Vehicle System Dynamics* **21,** 269–296.

Roberts, J. B. and Spanos, P. D., 1990, *Random Vibration and Statistical Linearization,* Wiley, New York.

Sharp, R. S. and Hassan, A. S., 1986, "The relative performance capabilities of passive, active and semi-active car suspensions," *Proceedings of Institution of Mechanical Engineers* **20(D3)**, 219–228.

Shinozuka, M., 1972, "Monte Carlo solution of structural dynamics," *Computers & Structures* **2**, 855–874.

Shinozuka, M. and Deodatis, G., 1991, "Simulation of stochastic processes by spectral representation," *Applied Mechanics Reviews* **44**, 191–204.

Surace, C., Worden, K., and Tomlinson, G. R., 1992, "An improved nonlinear model for an automotive shock absorber," *Nonlinear Dynamics* **3**, 413–429.

Verros, G. and Natsiavas, S., 2001, "Dynamics of vehicles with semi-active suspensions exhibiting wheel hop," *Vehicle System Dynamics (Supplement)* **35**, 135–148.

Verros, G., Goudas, H., Natsiavas, S., and Hache, M., 2000a, "Dynamics of large scale vehicle models," in *Proceedings of the 2000 International ADAMS Conference*, Orlando, FL.

Verros, G., Natsiavas, S., and Stepan, G., 2000b, "Control and dynamics of quarter-car models with dual-rate damping," *Journal of Vibration and Control* **6**, 1045–1063.

Wallaschek, J., 1990, "Dynamics of non-linear automobile shock-absorbers," *International Journal of Non-Linear Mechanics* **25**, 299–308.